



to as  $X_{l+1}^{\text{orth}}$  in Ref. [1] Algorithm 1). This requires another SVD to obtain  $V^\dagger$ . This projection appears to be of little benefit, in fact it is not hard to construct examples where this could cause a problem. For example, consider an iteration of DMRG starting from an initial vacuum state  $|\cdots 00 \cdots\rangle$ , and suppose on the two sites corresponding to  $A$  and  $C$  the Hamiltonian contains some matrix element  $|10\rangle\langle 00|$ . In expanding the bond dimension of the  $A$  site, the state  $|1\rangle$  is clearly a good choice, and the state  $|10\rangle$  will be represented in the  $X_{\bar{A}}$  tensor. However the CBE algorithm projects out the kept states on the *right* site as well, meaning any state of the form  $|x0\rangle$  will be projected out, since  $|0\rangle$  will be one of the right singular vectors of  $C$ . Hence the state  $|10\rangle$  that should be included in the expanded basis will be missing. Important states that would appear in a 2-site DMRG update are therefore excluded. This is not a contrived example, as similar constructions appears in many constrained models such as gauge theories and quantum link models, typically with terms that span 3 sites (e.g., creation of a particle-antiparticle pair with an accompanying change in flux at a gauge site). In some cases the missing basis vectors would be included with additional DMRG sweeps, but this is less efficient and a real problem with TDVP[6] where such additional sweeps are not usually performed[7]. This problem can be avoided by simply omitting the projection onto the null space of  $C$ , and incidentally saving several  $O(dD^3)$  operations. We have not found any numerical examples where omitting this projection has a detrimental effect on the calculation.

Throughout the Letter, the authors refer to selecting expansion vectors from the orthogonal two-site tangent space, referred to as DD, the space of states that are discarded both on the  $A$  site and the  $C$  site[8]. However the left singular vectors of  $X_{\bar{A}}$  cannot be separated into components that are kept (or not) with respect to site  $C$ . In order to split the tensor  $X$  into 2-site spaces KK, KD, DK, DD, we need to first shift the orthogonality center onto the bond, by factorizing  $C = \Lambda B$ , where  $B$  is right orthogonalized and  $\Lambda$  lives on the bond between  $A$  and  $B$ . Extending this bond basis with the null spaces  $\bar{A}$  and  $\bar{B}$  gives the 2-site tangent spaces as the four different combinations of  $(A \oplus \bar{A}) \otimes (B \oplus \bar{B})$ . Expansion vectors from  $\bar{A}$  cannot be selected by whether they belong (or not) to  $\bar{B}$ , since they are separate Hilbert spaces and that information is lost when taking the tensor product. The Hilbert space that will be optimized in the DMRG iterations is the  $(D+k) \times dD$ -dimensional space of  $(A \oplus \tilde{A}) \otimes (B \oplus \bar{B})$ , where  $\tilde{A} \subseteq \bar{A}$  is the carrier space of the  $k$  expansion vectors. Writing the expansion tensor  $X$  in partitioned form,

$$X = \begin{pmatrix} X_{\text{KK}} & X_{\text{KD}} \\ X_{\text{DK}} & X_{\text{DD}} \end{pmatrix}, \quad (4)$$

the states already contained in  $A$  are the top rows of  $X$ ,  $(X_{\text{KK}} \ X_{\text{KD}})$ . Candidate expansion vectors come from the bottom rows, being the null space  $\bar{A}$ . This

corresponds to the SVD of the  $(d-1)D \times dD$  matrix  $(X_{\text{DK}} \ X_{\text{DD}})$ . CBE chooses to only consider the component  $X_{\text{DD}}$  by projecting onto the discarded states  $\bar{B}$ , which sets  $X_{\text{DK}}$  to zero prior to the SVD. This throws away potentially useful information that could be used to improve the basis, and does not have the effect that the authors suggest.

**Randomized SVD** – Instead of using shrewd selection[1] to approximate the contraction of Eq. (2), a more efficient and accurate way to obtain the  $k$  dominant singular values of  $X_{\bar{A}}$  is via the Randomized SVD (RSVD)[3]. the RSVD has already been used to accelerate 2-site DMRG[9], and other algorithms[10–12]. The core of the RSVD is the *range finding algorithm* for finding an approximate span of the dominant singular vectors of a matrix. To find the span of the dominant  $k$  left singular vectors of  $X_{\bar{A}}$ , we multiply it by a Gaussian random matrix  $\Omega$  of dimension  $dD \times k$ . We then perform a  $QR$  decomposition,

$$QR = X_{\bar{A}}\Omega, \quad (5)$$

where  $Q$  is a  $dD \times k$  left-orthogonal matrix and  $R$  is  $k \times k$  upper triangular.  $Q$  contains an approximation of the dominant left singular vectors of  $X_{\bar{A}}$ . If we only need  $k$  *approximate* singular vectors then we can stop here. But while the leading singular vectors should be represented quite accurately, the tail of the spectrum will not be accurate. To obtain an accurate spectrum for all  $k$  singular values, the RSVD algorithm uses the range finding algorithm to firstly find a larger set of vectors  $k+p$ , where  $p$  is the *oversampling parameter* ( $p=10$  is typical)[3]. Once we have  $Q$  as a  $dD \times (k+p)$  dimensional matrix, we project the original matrix  $X_{\bar{A}}$  into this space and perform an SVD,

$$UDV^\dagger = Q^\dagger X_{\bar{A}}, \quad (6)$$

where  $D$  is the diagonal matrix of singular values,  $U$  is left-orthogonal, and  $V^\dagger$  is right-orthogonal. Projecting  $U$  onto the  $k$  largest singular values,  $QU$  now contains the  $k$  dominant singular vectors of  $X_{\bar{A}}$  with high accuracy. However we have found that this step is often not necessary, and in our numerical experiments the range finding algorithm works quite well and is very cheap as it requires just one tensor network contraction and one  $QR$  decomposition. The reason that the range finding works so well is that the selection of states to use as expansion vectors is not very sensitive, and in fact *random* vectors work reasonably well, as shown below, and also used to good effect by Oseledets and Dolgov[13]. Range finding can be seen as a semi-random algorithm that improves upon purely random vectors. RSVD interpolates between range finding for  $p \rightarrow 0$ , becoming equivalent to the exact SVD when  $k+p$  is equal to the rank of  $X_{\bar{A}}$ . Importantly, the computational complexity of the RSVD and range finding algorithms are dominated by the matrix-matrix



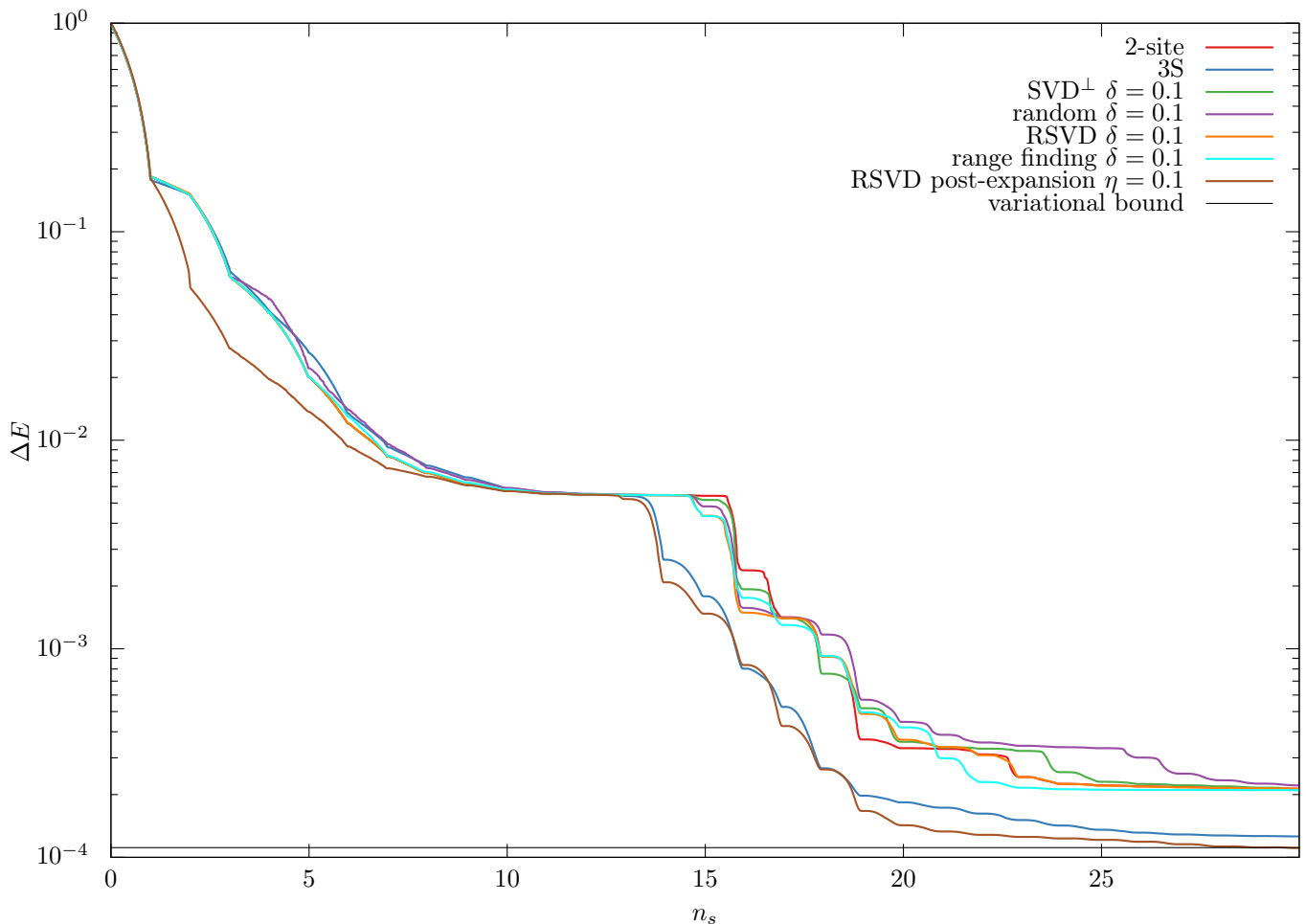


FIG. 1. Convergence in the relative error for non-interacting fermions with PBC, otherwise same parameters as used in Ref. [1] Fig. S-6 with bond dimension  $D = 600$ . 3S result uses a mixing parameter of  $\alpha = 10^{-4}$ .  $\text{SVD}^\perp$  is a baseline comparison against CBE, using a full SVD of the tensor  $X_{\bar{A}}$  projected onto the 2-site tangent space. *Random* uses  $k = \delta D$  Haar-distributed random vectors. *RSVD* and *range finding* are the  $O(dwkD^2)$  algorithms discussed in the main text. *RSVD post-expansion* uses a new variant of 3S where  $k = \eta D$  expansion vectors are added to the MPS after the truncation step. The *variational bound* is the best energy we could obtain for fixed bond dimension  $D = 600$ . In the first half of the calculation, the 2-site and  $\text{SVD}^\perp$  lines are hidden by that of RSVD, which in turn is mainly hidden by the range finding curve.

want to improve the relative error then it is much better to simply increase the bond dimension a few percent. That is, the best performance is obtained by *continuing to increase the bond dimension*, only stopping once the desired error is achieved. For most purposes the resulting wavefunction is good enough, but if a specific calculation requires something closer to the variational bound for a lower bond dimension, then it is often better to approach the variational energy from *below*, starting from a larger bond dimension and progressively reducing it, perhaps combined with a small mixing term (or bond expansion) that is smoothly taken to zero at the same time. The authors own comparisons of CBE versus 3S in figures S-7 and S-8 demonstrate this: the most efficient way to get to a given relative error is to continue increasing the bond dimension until the desired energy error is achieved. It

is in this sense that 3S is much more efficient than 2-site DMRG[4]. It is surely true that CBE is more efficient than 3S in systems with short-range interactions, but the authors own calculation in figure S-7 shows that the difference is small: although there is a long tail for 3S to converge for a fixed bond dimension, this is entirely expected and the important message of figure S-7 is that the most efficient way to lower the variational energy is to continue increasing the bond dimension. Indeed, the figure shows that this only takes *one additional sweep* with increased bond dimension, with computational resources that are only slightly higher than CBE. We note that the authors recommend using 3S-style mixing in the early stages of a calculation anyway[22], but in some cases this isn't enough and the mixing is required throughout.

None of the example calculations presented in Ref. [1]

contain interactions beyond 6 sites. It has been understood for a long time[4, 17] that 2-site DMRG (and hence also CBE and other algorithms based on expanding the environment bond prior to the optimization step; we refer to this class of algorithm as *local pre-expansion*) can have convergence problems with long range interactions. To illustrate this, we take an example from Ref. [1], for spinful non-interacting fermions on an  $L = 100$  site chain but now making the boundary condition *periodic*, and pre-expansion algorithms struggle to converge. This is shown in Fig. [1], where we compare several variants of pre-expansion including 2-site DMRG and the randomized SVD approach described above, and density matrix mixing via the 3S algorithm[4]. All of the algorithms get temporarily stuck in a metastable excited state, which corresponds to the *open* boundary condition wavefunction. It takes some time for the basis to grow sufficiently to contain Hamiltonian matrix elements that connect the periodic boundary, and thereafter the convergence resumes. But even after overcoming the metastable state, local bond expansion algorithms have trouble, often encountering additional metastable plateaus, and none of the local expansion algorithms get the relative error closer than a factor  $\sim 2$  of the variational bound for  $D = 600$  after 30 sweeps. However it is notable that all of the presented algorithms, including random expansion vectors, converge very well in the initial steps, indicating that in the absence of long range interactions the choice of algorithm is not a decisive factor. This is not a detail of our particular implementation of DMRG, and we verified that the behavior of the 2-site DMRG code in the iTensor toolkit[23] is consistent with these results[24]. The algorithms escape from the metastable state rather chaotically, and this depends very sensitively on the numerical details. For example, decreasing the  $\epsilon$  tolerance of the eigensolver might help the calculation to escape the metastability, or it might cause the calculation to fall even deeper into the metastable state. We don't know of any systematic way to tune these parameters in this situation, so we simply used the recommended default parameters used by the Matrix Product Toolkit[25]. The *random*, *RSVD*, and *range finding* algorithms use randomized sketching and are therefore non-deterministic; for these cases we ran 10 instances of the same calculation and chose a sample that best represents the median convergence. The separate runs produce near-identical results for the first half of the calculation, and only differ once they escape the metastable state. However the distribution of the results for each algorithm is quite distinct such that the depiction in Fig. [1] is representative of the expected relative performance. Fig. [1] also includes a calculation using *post-expansion*, which is a term we use to describe the class of algorithms that expand the basis after the optimisation step. This class includes the 3S algorithm as well as a new algorithm that uses the randomized SVD of the 3S mixing term to construct  $k$

expansion vectors in the null space of  $C$ , which are added basis after the truncation giving an MPS with a bond dimension of  $D + k$ . This can also be done in computation time  $O(dwkD^2)$ , and has an appealing physical interpretation. Full details of these algorithms will be published separately[26].

I.P.M. acknowledges funding from the National Science and Technology Council (NSTC) Grant No. 122-2811-M-007-044. The calculations presented here were obtained using the Matrix Product Toolkit[25].

## Appendix A: Additional details and benchmarks

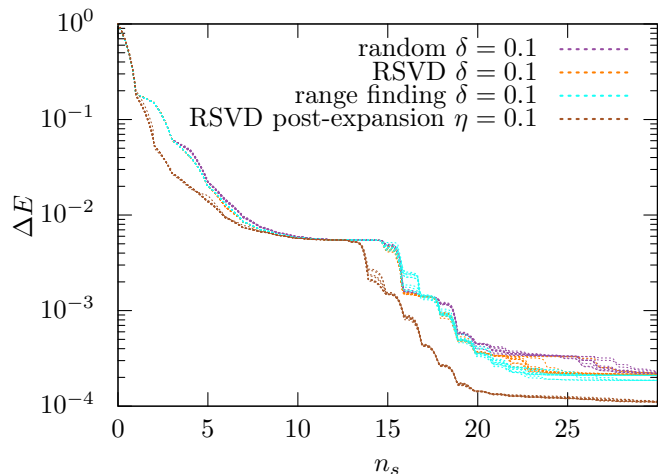


FIG. 2. All runs of the randomized algorithms from Fig. [1].

In Fig. [1], four of the algorithms are based on randomized sketching (*random*, *RSVD*, *range finding*, *RSVD post-expansion*). While the performance of these algorithms is generally not random, the escape from a metastable state is rather chaotic and small changes can affect the calculation, even for notionally deterministic algorithms. To obtain Fig. [1] for the randomized algorithms, we ran each calculation 10 times and selected one run that we thought best represented the median performance. We show all of the runs in Fig. [2]. Four out of the ten runs using the range finding algorithm actually found a lower energy state than 2-site DMRG, showing that some randomness can help escape metastability, even though the 2-site algorithm is exploring a larger local Hilbert space.

Fig. [3] shows the CPU time for the 3S, pre-expansion and post-expansion algorithms. Calculations were performed on a single core Intel Core i7-12700KF CPU[27], with double precision complex arithmetic[28]. With the local Hilbert space dimension of 3 multiplets, the  $O(d)$  vs  $O(d^2)$  performance improvement of the new algorithms is not large. We argue in the main text that the most relevant performance comparison is during the bond growth

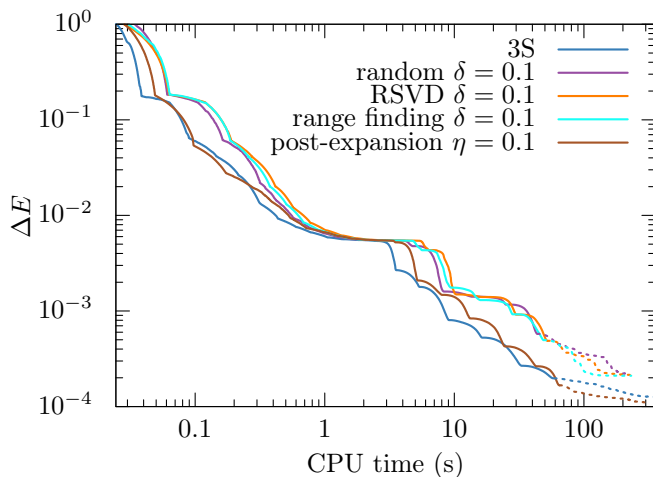


FIG. 3. Log-log plot of the relative error in the energy versus CPU time in seconds for the 3S, pre-expansion and post-expansion algorithms from Fig. [1]. Solid lines are the bond expansion phase, as the bond dimension  $D$  is increased to 600. Dashed lines are a further 11 sweeps with  $D = 600$ .

phase of the calculation, which is indicated in solid lines, transitioning to dashed lines for the final part of the calculation with fixed  $D$ .

## Appendix B: Hubbard-Holstein model

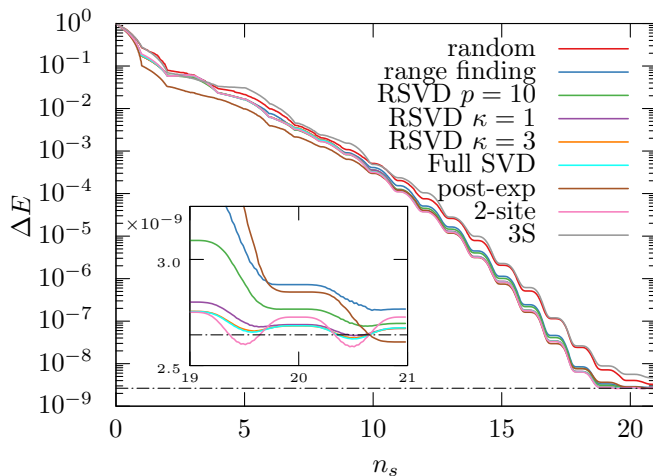


FIG. 4. Convergence of the Hubbard-Holstein model, energy versus number of half-sweeps. The random, range finding, and RSVD algorithms all use  $\delta = 0.1$  bond expansion. Post-exp is post-expansion using RSVD with  $p = 10$  oversampling. The inset shows the detailed convergence over the last two sweeps where the bond dimension is fixed at  $D = 600$ . The black dashed line is an estimated variational bound for  $D = 600$ . Post-expansion adds  $\eta = 0.1$  expansion states after the truncation phase, leading to an MPS with a final bond dimension of  $D(1 + \eta) = 660$ .

As a second benchmark, we examine the Hubbard-Holstein model, using the same parameters as Fig. 3 of Ref. [1], with maximum phonon occupancy of 3. Focusing on bond dimension  $D = 600$ , Fig. [4] shows the relative energy error per sweep for a selection of different local pre-expansion algorithms. *Full SVD* is a baseline comparison using the full SVD of the expansion tensor  $X_{\bar{A}}$  (note we did *not* project out the kept states of the  $C$  tensor). *Random* vectors do not work so well in this model, probably because of the large local Hilbert space dimension of 12 states means that the  $k = 0.1D = 60$  expansion states out of a possible 660 has a relatively low probability of making a good selection. The *range finding* algorithm works very well though. Note that for the random and range finding algorithms, we force a minimum of 1 state per quantum number sector into the expansion basis. Without sampling all of the available symmetry sectors, the random and range finding algorithms are ineffective. We also show three settings for oversampling of the RSVD; the baseline  $p = 10$  oversampling suggested in Ref. [3], and multiplicative oversampling with  $p = \min(k + 10, \kappa k)$ , for  $\kappa = 1$  and  $\kappa = 3$ . Multiplicative oversampling has a theoretical truncation error of a factor  $\simeq 1 + 1/\kappa$  larger than the exact SVD[3], and  $\kappa = 1$  is more than sufficient for this calculation. We also show 3S and 2-site DMRG results for comparison. Aside from the *random* and *3S* curves, the remaining curves are basically on top of each other. The inset shows the detail of the convergence in the final sweeps. For pre-expansion algorithms, the energy can drop below the variational bound for  $D = 600$  because of the larger Hilbert space during the bond expansion, which leads to a shallow bound state and a lower energy at that bond[19, 20]. At the end of the sweep, when all of the MPS bonds are dimension  $\leq 600$ , the energy is above the estimated variational bound. Because the RSVD post-expansion algorithm results in an MPS with an enlarged bond dimension  $D(1 + \eta)$ , it is allowed that the final energy is below the estimated variational bound and this actually occurs at the end of the calculation.

For completeness, we show the CPU time for the Hubbard-Holstein calculation in Fig. [5]. All of the pre-expansion and post-expansion algorithms perform similarly. 3S suffers from the larger local Hilbert space due to the  $O(d^2)$  scaling. Random pre-expansion has a somewhat worse energy, and post-expansion is somewhat slower because both sides of the active tensor have an expanded bond dimension, i.e., in pre-expansion on a right-to-left sweep the  $C$  tensor has dimension  $(D + k) \times d \times D$ , but for post-expansion it has dimension  $(D + k) \times d \times (D + k)$ . However, post-expansion has a significant advantage, in that it works well even when there are long-range interactions. For the Hubbard-Holstein model this means that it is possible to factorize the unit cell of the lattice into separate fermion and phonon sites, which enables a significant increase the

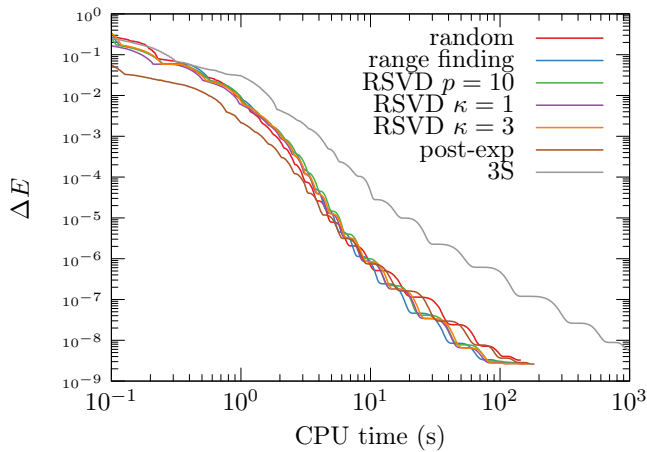


FIG. 5. CPU time (seconds) for the Hubbard-Holstein model.

number of phonon modes. With  $d_{\text{ph}}$  phonon modes (corresponding to a maximum phonon occupancy of  $d_{\text{ph}} - 1$ ), the coarse-grained lattice site has a local Hilbert space of  $3d_{\text{ph}}$  multiplets ( $4d_{\text{ph}}$  without using  $SU(2)$  symmetry for the fermions), whereas splitting the unit cell into two lattice sites gives one site for 3 fermion states and one site for the  $d_{\text{ph}}$  phonon modes. In principle the CPU time is then proportional to  $3 + d_{\text{ph}}$ , rather than  $3d_{\text{ph}}$ . To tackle even larger values of  $d_{\text{ph}}$ , the phonon modes can themselves be factorized into multiple sites[29]. Unfortunately, this procedure fails completely for local pre-expansion algorithms, including 2-site DMRG, because on every pair of neighboring lattice sites there is only at most one fermion site, and hence expanding the bond cannot introduce new fermionic quantum numbers.

On increasing the maximum number of phonons, the advantage of using a fine-grained unit cell becomes very clear. Fig. [6] shows the convergence for the same calculation as Fig. [4] but now with up to 8 phonons per site ( $d_{\text{ph}} = 9$ ). Using a unit cell of two sites, there are now a total of 100 sites in the lattice (50 fermion sites and 50 phonon sites), and post-expansion works extremely well, producing an energy that is nearly as good as for the coarse-grained lattice. Splitting the fermion and phonon sites slightly restricts the entanglement allowed between them compared with the coarse-grained lattice, which affects the energy slightly. This can be compensated by increasing the bond dimension, and  $D = 680$  is sufficient here. Pre-expansion algorithms, including 2-site DMRG, fail completely with the factorized basis.

The CPU time for this calculation is shown in Fig. [7], which shows the expected  $\simeq 2$  speedup from using a factorized basis, going from local Hilbert space sizes of  $3 \times 9 = 27$  to  $3 + 9 = 12$ . This advantage clearly gets bigger for even larger phonon numbers needed for the Holstein model when the zero mode is not removed from the basis[29, 30].

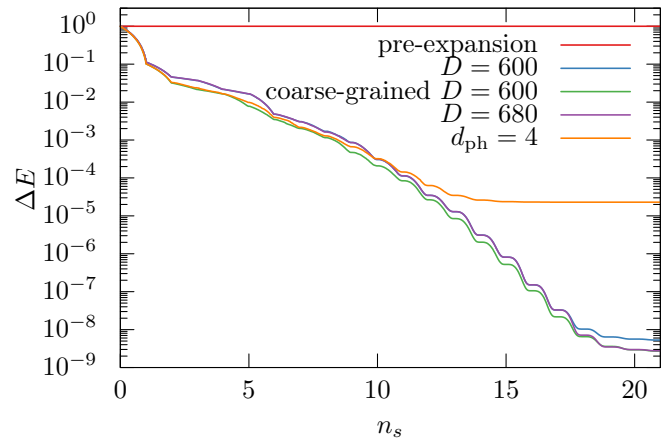


FIG. 6. Convergence of the Hubbard-Holstein model increasing the maximum phonon number to 8 ( $d_{\text{ph}} = 9$  phonon modes). For comparison purposes, the  $D = 600$  result for 3 phonons ( $d_{\text{ph}} = 4$ ) is included showing that the limiting factor affecting the ground state energy is the number of phonon modes. The coarse-grained curve uses the basis of the combined fermion+phonon. All pre-expansion algorithms fail completely and the energy stays at 0.

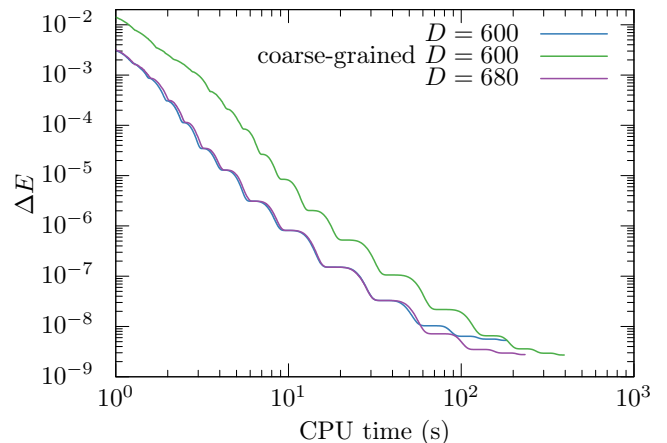


FIG. 7. CPU time for the calculation of Fig. [6].

### Appendix C: Random sketching versus shrewd selection

In this section, we compare in detail the effectiveness of the algorithms based on random sketching. In Fig. [8] (a), we compare the singular values of the expansion tensor  $X$  with and without the projection onto the 2-site tangent space, for bond dimension  $D = 300$  at the center of the  $L = 20$  site chain. The projection makes very little difference to the top part of the spectrum, except to give very low weight to some states that would otherwise appear around the middle of the spectrum. The bulk of the spectrum has a very steady exponential decay, which explains why random expansion vectors work so well: a Haar random vector has an expected weight

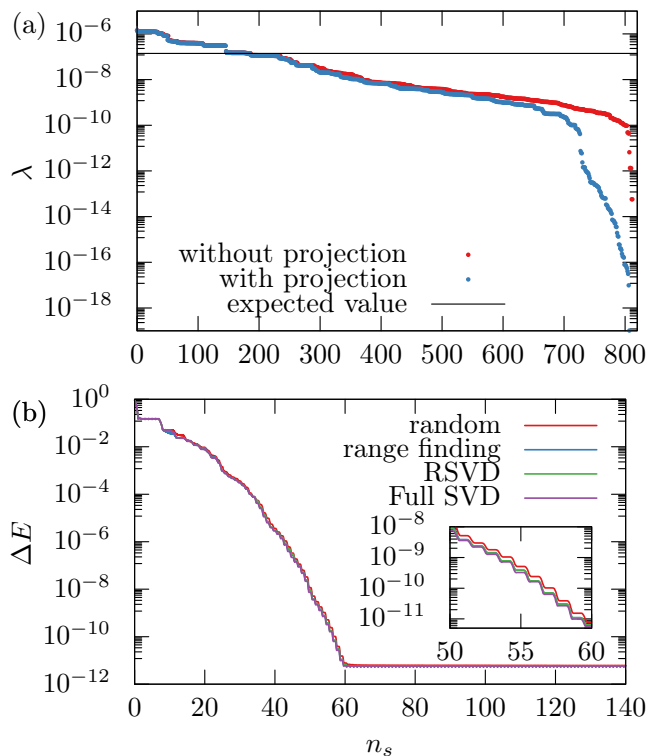


FIG. 8. Comparison using randomized sketching for the expansion vectors using the same parameters as figure S-5 of Ref. [1]. (a) the singular values of the expansion matrix  $X$  without projecting onto the two-site tangent space and  $X_{\bar{A}}$  with the projection. (b) difference in the variational energy from the exact solution, starting from a  $D = 1$  valence bond state increasing to  $D = 300$ . The curve for the range finding algorithm is almost indistinguishable from (and hidden by) the RSVD curve. For the RSVD, we used oversampling factor  $\kappa = 1$ , with a minimum oversample of 10.

of nearly 10% of the leading singular value. Fig. [8] (b) shows the convergence of the energy for the different algorithms. The full SVD is included as a baseline. As expected from the unchanged top part of the spectrum in Fig. [8] (a), it makes no difference in this case whether the expansion tensor is projected onto the two-site tangent space or not. As best as we can tell, random vectors are already very close to the ‘moderate pre-selection’ line of figure S-5 of Ref. [1], and range-finding exceeds it. However random vectors are much less effective when only a few states from the local Hilbert space are used, such as the Hubbard-Holstein model. In that case, the phonon number distribution is far from uniform, and only a small subset of the null space are effective expansion vectors and we recommend that at least range-finding is used, and preferably the RSVD. When using good quantum numbers, there is a question of how to choose the quantum number sectors of the expanded states. Our approach is to choose sectors such that the distribution of quantum numbers matches the the states already kept,

and in addition we require at least one expansion vector in each available quantum number sector. This typically results in slightly more than  $\delta D$  expansion vectors, but the cost of this is negligible as the computation time is dominated by the matrix multiplies in the largest quantum number sectors. For the post-expansion algorithm, this requirement to explore all candidate quantum number sectors means that random vectors or random range-finding algorithms are not so effective, since there is no singular value truncation to control the number of quantum number sectors, which can therefore get very large. For this reason, we recommend using the RSVD with post-expansion, since the singular value selection serves to prevent the number of quantum number sectors from growing out of control. But even without quantum number symmetries, it is best to use the RSVD with post expansion. This is because in post-expansion the vectors are used for the entire sweep so it is more important that the vectors are chosen as to have a high probability of contributing to the converged wavefunction. In contrast, in the pre-expansion algorithm the vectors are selected from the null space of the environment tensor and they are discarded at the end of the current iteration, so a single iteration with an unlucky or poor selection of expansion vectors is of no major consequence, as long as there is a good average selection throughout multiple sweeps.

\* [ian@phys.nthu.edu.tw](mailto:ian@phys.nthu.edu.tw)

† [j.osborne@uqconnect.edu.au](mailto:j.osborne@uqconnect.edu.au)

- [1] A. Gleis, J.-W. Li, and J. von Delft, Controlled bond expansion for density matrix renormalization group ground state search at single-site costs, *Phys. Rev. Lett.* **130**, 246402 (2023).
- [2] We use  $k$  rather than  $\tilde{D}$  for clarity of notation.
- [3] N. Halko, P. G. Martinsson, and J. A. Tropp, Finding structure with randomness: Probabilistic algorithms for constructing approximate matrix decompositions, *SIAM Review* **53**, 217 (2011), <https://doi.org/10.1137/090771806>.
- [4] C. Hubig, I. P. McCulloch, U. Schollwöck, and F. A. Wolf, Strictly single-site dmrg algorithm with subspace expansion, *Phys. Rev. B* **91**, 155115 (2015).
- [5] V. Zauner-Stauber, L. Vanderstraeten, M. T. Fishman, F. Verstraete, and J. Haegeman, Variational optimization algorithms for uniform matrix product states, *Phys. Rev. B* **97**, 045145 (2018).
- [6] J. Haegeman, J. I. Cirac, T. J. Osborne, I. Pižorn, H. Verschelde, and F. Verstraete, Time-dependent variational principle for quantum lattices, *Phys. Rev. Lett.* **107**, 070601 (2011).
- [7] J. Haegeman, C. Lubich, I. Oseledets, B. Vandereycken, and F. Verstraete, Unifying time evolution and optimization with matrix product states, *Phys. Rev. B* **94**, 165116 (2016).
- [8] Abstract: CBE identifies parts of the orthogonal space carrying significant weight in  $H\Psi$  and expands bonds to include only these. Page 2, final paragraph: The first in-



- sight is that the subspace of DD relevant for lowering the GS energy is relatively small [...] When expanding a bond, it thus suffices to add only this small subspace (hence the moniker controlled bond expansion), or only part of it, to be called relevant<sub>DD</sub> ( $r_{DD}$ ). Also the following discussion onto page 3. Footnote [29]: If 2s DMRG has converged to an optimal MPS  $\Psi_D$  with fixed bond dimension  $D$ , the size of  $r_{DD}$  is zero.
- [9] L. Kohn, F. Tschirsich, M. Keck, M. B. Plenio, D. Tamascelli, and S. Montangero, Probabilistic low-rank factorization accelerates tensor network simulations of critical quantum many-body ground states, *Phys. Rev. E* **97**, 013301 (2018).
- [10] D. Tamascelli, R. Rosenbach, and M. B. Plenio, Improved scaling of time-evolving block-decimation algorithm through reduced-rank randomized singular value decomposition, *Phys. Rev. E* **91**, 063306 (2015).
- [11] S. Morita, R. Igarashi, H.-H. Zhao, and N. Kawashima, Tensor renormalization group with randomized singular value decomposition, *Phys. Rev. E* **97**, 033310 (2018).
- [12] K. Batselier, W. Yu, L. Daniel, and N. Wong, Computing low-rank approximations of large-scale matrices with the tensor network randomized svd, *SIAM Journal on Matrix Analysis and Applications* **39**, 1221 (2018), <https://doi.org/10.1137/17M1140480>.
- [13] I. V. Oseledets and S. V. Dolgov, Solution of linear systems and matrix inversion in the tt-format, *SIAM Journal on Scientific Computing* **34**, A2718 (2012), <https://doi.org/10.1137/110833142>.
- [14] The projection to remove the right singular vectors could also be done with the same cost, however the SVD to obtain these singular vectors is relatively expensive, at a cost of  $O(dD^3)$ .
- [15] F. Verstraete, D. Porras, and J. I. Cirac, Density matrix renormalization group and periodic boundary conditions: A quantum information perspective, *Phys. Rev. Lett.* **93**, 227205 (2004).
- [16] S. Russell and P. Norvig, *Artificial Intelligence: A Modern Approach*, 3rd ed. (Prentice Hall, 2010).
- [17] S. R. White, Density matrix renormalization group algorithms with a single center site, *Phys. Rev. B* **72**, 180403 (2005).
- [18] S. V. Dolgov and D. V. Savostyanov, Alternating minimal energy methods for linear systems in higher dimensions, *SIAM Journal on Scientific Computing* **36**, A2248 (2014), <https://doi.org/10.1137/140953289>.
- [19] J. Dukelsky, M. A. Martín-Delgado, T. Nishino, and G. Sierra, Equivalence of the variational matrix product method and the density matrix renormalization group applied to spin chains, *Europhysics Letters* **43**, 457 (1998).
- [20] I. P. McCulloch and M. Gulácsi, Comment on “equivalence of the variational matrix product method and the density matrix renormalization group applied to spin chains” by j. dukelsky et al., *Europhysics Letters* **61**, 138 (2003).
- [21] This does not violate the variational principle, because only the *total* energy of the entire system is variational. If one bond has an energy below that of the ground state it will be compensated by higher bond energies elsewhere. This is why DMRG with bond expansion never reaches the exact variational minimum for fixed bond dimension[15].
- [22] Section S-3(B), final paragraph.
- [23] M. Fishman, S. R. White, and E. M. Stoudenmire, The ITensor Software Library for Tensor Network Calculations, *SciPost Phys. Codebases*, 4 (2022).
- [24] As iTensor does not support non-Abelian symmetries, we used a  $U(1) \times U(1)$  basis for the iTensor calculations. This is not directly comparable to the  $U(1) \times SU(2)$  results shown here, but the qualitative behavior is the same.
- [25] The matrix product toolkit, <https://github.com/mptoolkit>.
- [26] I. P. McCulloch and J. Osborne, in preparation.
- [27] According to the GeekBench 6 benchmark at <https://browser.geekbench.com> this processor has approximately 89% faster single-core performance than the i7-9750H CPU used in Ref. [1].
- [28] Although though the Hamiltonian is purely real, our code currently only allows complex arithmetic, and we used complex Gaussian random matrices. In principle, real arithmetic would be  $\sim 3$ -4 times faster.
- [29] E. Jeckelmann and S. R. White, Density-matrix renormalization-group study of the polaron problem in the holstein model, *Phys. Rev. B* **57**, 6376 (1998).
- [30] F. Dorfner, L. Vidmar, C. Brockt, E. Jeckelmann, and F. Heidrich-Meisner, Real-time decay of a highly excited charge carrier in the one-dimensional holstein model, *Phys. Rev. B* **91**, 104302 (2015).